AMERICAN METEOROLOGICAL SOCIETY

Journal of Climate

EARLY ONLINE RELEASE

The DOI for this manuscript is doi: 10.1175/JCLI-D-13-00017.1

Interhemispheric teleconnections from tropical heat sources in intermediate and simple models

X. Ji[1], J. D. Neelin[1], S.-K. Lee[2] and C. R. Mechoso[1]

[1]*Department of Atmospheric and Oceanic Sciences, University of California, Los Angeles, California, USA*

[2]*Cooperative Institute for Marine and Atmospheric Studies, University of Miami, and NOAA/Atlantic Oceanographic and Meteorological Laboratory, Miami, Florida*

Corresponding author address: J. David Neelin, Department of Atmospheric and Oceanic Sciences, 7127 Math Science Building, UCLA, 405 Hilgard Avenue, Los Angeles, California, 90095-1565, USA.
E-mail: neelin@atmos.ucla.edu

Abstract

The mechanisms that control the interhemispheric teleconnections from tropical heat sources are investigated using an intermediate complexity model (a Quasi-Equilibrium Tropical Circulation Model, QTCM) and a simple linear two-level model with dry dynamics. Illustrating the interhemispheric teleconnection process with an Atlantic Warm Pool principal case, the heat source directly excites a baroclinic response that spreads across the equator. Three processes involving baroclinic-barotropic interactions—shear advection, surface drag, and vertical advection—then force a cross-equatorial barotropic Rossby wave response. An analysis of these processes in QTCM simulations indicates that: (1) shear advection has a pattern that roughly coincides with the baroclinic signal in the tropics and subtropics; (2) surface drag has large amplitude and spatial extent, and can be very effective in forcing barotropic motions around the globe; (3) vertical advection has a significant contribution locally and remotely where large vertical motions and vertical shear occur. The simple model is modified to perform experiments in which each of these three mechanisms may be included or omitted. By adding surface drag and vertical advection, and comparing each to shear advection, the effects of the three mechanisms on the generation and propagation of the barotropic Rossby waves are shown to be qualitatively similar to the results in QTCM. It is also found that the moist processes included in the QTCM can feed back on the teleconnection process and alter the teleconnection pattern by enlarging the prescribed tropical heating in both intensity and geographical extent, and by inducing remote precipitation anomalies by interaction with the basic state.

1. Introduction

Tropical heat sources can remotely influence ocean basins and continents through atmospheric teleconnections (e.g., Horel and Wallace 1981; Ropelewski and Halpert 1987; Wallace et al. 1998; Trenberth et al. 1998). In addition to many teleconnection studies in general circulation models (GCMs; e.g., Lau 1985; Mechoso et al. 1987; Kumar and Hoerling 1998; Barnston et al. 1999; Goddard and Graham 1999; Latif et al. 1999; Saravanan and Chang 2000), much has been learned from simpler models. In the tropics, heating anomalies directly force a baroclinic signal that tends to remain trapped in latitude. Thus, highly damped shallow water models (Matsuno 1966; Webster 1972; Gill 1980), which assume a vertical structure of a single deep baroclinic mode, can give a plausible first approximation to the low-level wind field in the vicinity of heating anomalies. In mid-and high-latitudes, teleconnections tend to be dominated by an equivalent barotropic signal for two reasons. Firstly, barotropic stationary or low-frequency Rossby waves in westerly flow tend to be less equatorially trapped than their baroclinic counterparts (Salby and Garcia 1987). Secondly, vertical propagation tends to reduce the contribution of baroclinic modes in the mid-latitude troposphere, leaving the signal far from the source dominated by an equivalent barotropic mode (Held et al. 1985). Thus barotropic models have been widely used to study the teleconnection response at midlatitudes (e.g., Hoskins and Karoly 1981; Simmons 1982; Simmons et al. 1983; Held and Kang 1987). However, since the heating does not directly force a barotropic response, barotropic models used to study teleconnections must prescribe a vorticity source or "Rossby wave source" (Sardeshmukh and Hoskins 1988), which can be based, for instance, on baroclinic divergence at upper levels or on baroclinic transient motions diagnosed from a GCM simulation (Held and Kang 1987). This diagnosed Rossby wave source is one convenient approach that permits the barotropic processes

to be examined while deferring investigation of the complex baroclinic to barotropic pathway in the tropics-to-midlatitudes teleconnection process. However, many of the terms that are specified as a fixed source in this approach are dynamical quantities whose scales, spatial form etc. depend on the interaction of the baroclinic mode with the basic state in ways that can be interesting to elucidate. Multi-level linear, steady-state wave models with both baroclinic and barotropic components comprise part of a model hierarchy (Hoskins and Karoly 1981; Ting and Held 1990; DeWeaver and Nigam 2004) that can capture at least some aspects of the tropical-baroclinic to midlatitude-barotropic transition. Interactions with baroclinic transient eddies (Held et al. 1989; Hoerling and Ting 1994) can also alter the teleconnection pattern in a manner that is not easily captured by stationary wave models.

The energy exchange between equatorially trapped baroclinic modes and equivalent barotropic modes with a significant projection on midlatitudes needs, therefore, to be addressed in a more sophisticated way. Instead of prescribing a Rossby wave source based on upper level divergent flow in the one level barotropic vorticity equation (e.g., Sardeshmukh and Hoskins 1988, Held and Kang 1987), a series of studies have been examining this problem from the point of view of baroclinic-barotropic interaction terms and studying the effect of each mechanism at work in the baroclinic to barotropic transition. Majda and Biello (2003) develop a set of simplified asymptotic equations describing the nonlinear interaction of near-resonant long-wavelength barotropic wave trains and equatorial baroclinic wave trains in the presence of sheared zonal mean winds, and emphasize the central role of baroclinic mean shear for sufficiently rapid nonlinear exchange of energy between the tropics and midlatitudes. Biello and Majda (2004b) further examine this resonant nonlinear interaction in the presence of vertically and meridionally sheared zonal mean winds, i.e., including both meridionally symmetric and

antisymmetric (about the equator) vertical mean shear, and find that the effect of moderate antisymmetric winds is to shift the barotropic waves meridionally. Biello and Majda (2004a) incorporate the dissipative mechanisms arising from radiative cooling and atmospheric boundary layer drag, to explain how this mechanism creates barotropic/baroclinic spin up/spin down in the teleconnection process. Their results indicate that although the dissipation slightly weakens the tropics to midlatitude connection, strong localized wave packets are nonetheless able to exchange energy between barotropic and baroclinic waves on intraseasonal timescales in the presence of baroclinic mean shear. Wang et al. (2010) examine how, in the presence of background vertical shear, the transition from equatorial baroclinic mode to equivalent barotropic mode at midlatitudes establishes the interhemispheric influence of the Atlantic Warm Pool (AWP) in the northern hemisphere on the south eastern Pacific.

In this work, we aim at directly diagnosing and assessing the relative importance of the interaction terms between the baroclinic and barotropic modes that appear as source terms in the barotropic equation. These interaction terms are similar to a Rossby-wave source approach in that these terms appear as a vorticity source in the barotropic equation, but the "source" can be quantitatively and conceptually quite different than approaches based on upper level divergent flow in a single-level vorticity equation. For instance, if there is no vertical shear and no damping on the baroclinic mode associated with surface stress, then upper level divergence in the baroclinic mode does not produce any linear forcing of the barotropic mode. At the same time, by explicitly modeling the gravest baroclinic mode, the teleconnection pathway can be followed as the two modes interact, for instance with the baroclinic mode producing a teleconnection across the equator, and then interactions yielding a barotropic mode that can propagate to higher latitudes in the opposite hemisphere. Building on previous work with

idealized asymptotic equations, here we use realistic background states and more detailed physics including moist processes to analyze teleconnections arising from tropical heat sources.

We use two numerical models with different complexity, in both of which the baroclinic-barotropic interactions are explicitly formulated. The more complex one is a Quasi-Equilibrium Tropical Circulation Model (QTCM) (Neelin and Zeng 2000), in which part of the quasi-equilibrium convective closure is used to carry forward analytically the model solution for the baroclinic vertical structure in the convective regions. The full primitive equations are then projected on the resulting baroclinic plus barotropic basis functions for vertical structure. This intermediate complexity model retains some of the simplicity of the analytical solutions, while keeping full nonlinearity from the primitive equations, and a consistent representation of moist processes including a deep convective parameterization. The consistent vertical mode decomposition yields three mechanisms (Neelin and Zeng 2000) for excitation terms in the barotropic equations due to baroclinic terms: interactions of vertical shear in horizontal advection terms, vertical advection of vertically sheared motions, and interactions via surface stress in the boundary layer. The QTCM thus allows for quantifying the effect of each of those mechanisms, and to assess the role of feedbacks associated with moist processes. The simpler model we use is based on that of Lee et al. 2009), which is a two-level steady-state wave model linearized about background flows. In preparation for the present study, the Lee et al. (2009) version was extended to include the three mechanisms for excitation of barotropic modes present in the QTCM. The simple model permits experiments in which mechanisms may be included or omitted. Therefore, an assessment of individual impacts is obtained by retaining the forcing terms one at a time in the barotropic equation, and inspecting the differences in the teleconnection patterns obtained with each mechanism. Our primary focus is on the heat source

126 region above the Atlantic Warm Pool (AWP) because previous studies have shown that it has
127 significant interhemispheric influences (e.g., Wang et al. 2010).

128 The remainder of the text is organized as follows. Section 2 gives a brief introduction of
129 the two models as well as the modifications made for the study. Section 3 presents the QTCM
130 experiments, examines each of the three forcing terms of barotropic Rossby waves, and explores
131 the effect of moist feedback in the teleconnection process. Section 4 presents the simple model
132 experiments, narrowing down on the role of each forcing term. Section 5 consists of a summary
133 and discussion.

134

135 2. Models and Methodology

136 *a. QTCM*

137 The QTCM belongs in a class of tropical atmospheric model of intermediate complexity
138 that occupies a niche between GCMs and simple models. In the QTCM, the derivation from the
139 primitive equations is done systematically and the constraints placed on the baroclinic flow by
140 the GCM convective parameterizations with quasi-equilibrium (QE) thermodynamic closures are
141 exploited. Part of the QE convective closure can be used to carry forward analytically the model
142 solution for the vertical structure in convective regions. Using the vertical structures based on
143 these analytical solutions as the leading basis functions in a Galerkin projection of the primitive
144 equations, self-consistent nonlinear terms can be retained in advection, moist convection, and
145 vertical momentum transfer terms, among others. A more detailed model description can be
146 found in Neelin and Zeng (2000). The model performance has been analyzed in Zeng et al.
147 (2000) for climatology, and in Lin et al. (2000) and Lin and Neelin (2000, 2002) for

148 intraseasonal variability. Moist teleconnection mechanisms within the tropics have been
149 examined using this model in Su and Neelin (2002) and Neelin and Su (2005).

150 The present study uses the QTCM1 version 2.3 which retains a single basis function for
151 the vertical structure of temperature. This is the simplest configuration, but with considerable
152 success in capturing tropical phenomena, since the temperature structure matches the
153 consequences of a quasi-equilibrium convective scheme, and the baroclinic velocity basis
154 function is analytically compatible. This provides an appealing system for baroclinic-barotropic
155 decomposition. One might anticipate that an additional degree of freedom in the boundary layer
156 might alter some surface drag effects quantitatively. The numerical implementation of the
157 QTCM1 here covers the domain from 78.75°S to 78.75°N and over all longitudes, with a
158 horizontal resolution of 3.75° latitude and 5.625° longitude.

159 A brief review of the equation for the barotropic wind component in the QTCM is
160 presented below to aid the analysis of the barotropic teleconnection process in the following
161 sections. A summary of the QTCM1 equations are given for reference in Appendix. Using V_0 and
162 V_1 as the basis functions for velocity, the projected barotropic vorticity equation in Neelin and
163 Zeng (2000) is:

164 $$\partial_t \zeta_0 + curl_z(\mathcal{D}_{V0}(\mathbf{v_0}, \mathbf{v_1})) + \beta v_0 = -curl_z(\varepsilon_0 \mathbf{v_0}) - curl_z(\varepsilon_{10} \mathbf{v_1}) \qquad (1)$$

165 where subscripts 0 and 1 denote barotropic and baroclinic component, respectively, and
166 $\mathcal{D}_{V0}(\mathbf{v_0}, \mathbf{v_1})$, the operator containing nonlinear advection terms and horizontal diffusion is given
167 by:

168 $$\mathcal{D}_{V0}(\mathbf{v_0}, \mathbf{v_1}) = \mathbf{v_0} \cdot \nabla \mathbf{v_0} + \left\langle V_1^2 \right\rangle \mathbf{v_1} \cdot \nabla \mathbf{v_1} + \left\langle V_1^2 \right\rangle (\nabla \cdot \mathbf{v_1}) \mathbf{v_1} - K_H \nabla^2 \mathbf{v_0} \qquad (2)$$

where the term in brackets denote vertical averages over the troposphere $\langle X \rangle = p_T^{-1} \int_{p_{rt}}^{p_{rs}} X dp$. For the analysis of Rossby wave sources in the QTCM, we rearrange (1) to obtain:

$$\begin{aligned} &\partial_t \nabla^2 \psi_0' + curl_z(\mathbf{v}_0 \cdot \nabla \mathbf{v}_0)' - K_H \nabla^4 \psi_0' + \beta v_0' \\ &= -curl_z(\langle V_1^2 \rangle \mathbf{v_1} \cdot \nabla \mathbf{v_1})' - curl_z(\langle V_1^2 \rangle (\nabla \cdot \mathbf{v_1}) \mathbf{v_1})' - curl_z(\varepsilon_0 \mathbf{v_0} + \varepsilon_{10} \mathbf{v_1})' \end{aligned} \quad (3)$$

where ψ_0 is the barotropic stream function, and $()'$ denotes anomalies defined as the difference between a climatological run and a run with an imposed heating anomaly. The stationary barotropic Rossby wave response (i.e. of the l.h.s. of (3)) to a localized source is well known (e.g., Hoskins and Karoly 1981, Simmons et al. 1983; Held and Kang 1987) so we focus on the comparison of the forcing terms on the r.h.s. of (3). The three forcing sources of the barotropic motion that involve the interactions with baroclinic motion are defined as follows: 1) the shear advection term $-curl_z(\langle V_1^2 \rangle \mathbf{v_1} \cdot \nabla \mathbf{v_1})'$, which represents advective interactions of the baroclinic wind component (with vertical shear); 2) the vertical advection term $-curl_z(\langle V_1^2 \rangle (\nabla \cdot \mathbf{v_1}) \mathbf{v_1})'$, which represents the effect of vertical motion advecting the baroclinic wind component; 3) the surface drag term $-curl_z(\varepsilon_0 \mathbf{v}_0 + \varepsilon_{10} \mathbf{v}_1)'$, which derives from surface stress $-(g / p_T)\tau_s$ (with zero stress at model top) and a bulk formula parameterization $\tau_s = \tau|_{p_s} = \rho_a C_D V_s \mathbf{v_s}$. These three forcing mechanisms of the barotropic motion involved in the baroclinic-barotropic interactions are further discussed in section 3b in the teleconnection experiments. We further note that linearizing the interaction terms in (3) yields: $-curl_z(\langle V_1^2 \rangle \bar{\mathbf{v}}_\mathbf{1} \cdot \nabla \mathbf{v}_\mathbf{1}' + \langle V_1^2 \rangle \mathbf{v}_\mathbf{1}' \cdot \nabla \bar{\mathbf{v}}_\mathbf{1}) - curl_z(\langle V_1^2 \rangle (\nabla \cdot \mathbf{v}_\mathbf{1}') \bar{\mathbf{v}}_\mathbf{1} + \langle V_1^2 \rangle (\nabla \cdot \bar{\mathbf{v}}_\mathbf{1}) \mathbf{v}_\mathbf{1}') - curl_z(\varepsilon_0 \mathbf{v_0}' + \varepsilon_{10} \mathbf{v_1}')$. The linearized interaction terms make it clear that if there is no vertical shear or vertical velocity

in the mean state ($\bar{\mathbf{v}}_1 = 0$) and no drag on the baroclinic mode ($\varepsilon_{10} = 0$), then the baroclinic mode can have any vertical velocity ($\nabla \cdot \mathbf{v}_1'$), but there will be no forcing of the barotropic mode. This appears quite different from the assumptions used in traditional Rossby wave source approaches based on a vorticity equation at upper levels, but is similar in the sense that it diagnoses a vorticity source that drives the barotropic equation, in this case the equation for the full barotropic mode. We will refer to this as a "barotropic Rossby wave source" for clarity since it is the vorticity source term as it occurs projected on the full barotropic mode We also note that while we have retained the whole surface stress term on the right-hand side above, arguably it is more consistent to move the barotropic component of this, i.e., $-curl_z(\varepsilon_0 \mathbf{v}_0')$, to the l.h.s. in (3) since it acts as a drag on the barotropic mode. In that case the surface drag contribution to the barotropic Rossby wave source due to the baroclinic mode is simply $-curl_z(\varepsilon_{10} \mathbf{v}_1')$. We will show examples of both in diagnostics.

b. Simple model

The simple model we use in this study is based on that developed by Lee et al. (2009). This is a two-level model, in which equations are recast as baroclinic and barotropic components, and are linearized about prescribed background wind fields. The model is designed to simulate both the local and remote stationary response of the atmosphere when forced with a localized heating. In this model, the baroclinic response to tropical heating anomalies is essentially the same as described by the Matsuno-Gill model (Matsuno 1966; Gill 1980) with damping used in Lee et al (2009). This baroclinic response then excites a barotropic response by advective

interactions with vertical background wind shear (i.e., through the shear advection mechanism), and the barotropic signals are in turn transmitted to high latitudes.

Our modification of the Lee et al. (2009) model allows for consideration of surface drag as another mechanism of baroclinic-barotropic interactions. This was done by eliminating, from the relative vorticity equations, the linear momentum damping $-r\nabla^2\psi$ both in the upper (250mb) and lower (750mb) levels, and adding in the lower level a term $-r_s\nabla^2\psi$, where the surface drag coefficient is $r_s = (g/p_T)\rho_a C_D V_s$. Thus, in the barotropic and baroclinic vorticity equations, the linear damping coefficients r_0 and r_1 become $r_0 = r_1 = r_s/2$. We set $r_s = (3.5\text{day})^{-1}$ for $p_T = 500\text{mb}, C_D = 10^{-3}, V_s = 10\text{m s}^{-1}$. The simple model (as modified relative to Lee et al 2009) is thus given by the following barotropic and baroclinic vorticity equations:

$$\frac{1}{a\cos\theta}\left[\frac{\partial}{\partial\lambda}(\bar{u}_0\nabla^2\psi_0' + u_0'\nabla^2\bar{\psi}_0) + \frac{\partial}{\partial\theta}(\cos\theta\bar{v}_0\nabla^2\psi_0' + \cos\theta v_0'\nabla^2\bar{\psi}_0)\right] + 2\Omega\frac{v_0'}{a} \tag{4}$$
$$= -r_0\nabla^2\psi_0' + r_0\nabla^2\psi_1' + A_0\nabla^4\psi_0' + F_{\psi_0}$$

$$\frac{1}{a\cos\theta}\left[\frac{\partial}{\partial\lambda}(\bar{u}_1\nabla^2\psi_1' + u_1'\nabla^2\bar{\psi}_1) + \frac{\partial}{\partial\theta}(\cos\theta\bar{v}_1\nabla^2\psi_1' + \cos\theta v_1'\nabla^2\bar{\psi}_1)\right] + 2\Omega\frac{v_1'}{a} \tag{5}$$
$$= -r_1\nabla^2\psi_1' + r_1\nabla^2\psi_0' + A_1\nabla^4\psi_1' + F_{\psi_1}$$

where subscripts 0 and 1 denote barotropic and baroclinic mode respectively, variables are separated into the basic state and anomaly components denoted by bar and prime terms, A_0 and A_1 are the momentum diffusion coefficient for barotropic and baroclinic motion respectively. The differences from the model in Lee et al. (2009) are the two terms $r_0\nabla^2\psi_1'$ and $r_1\nabla^2\psi_0'$ that derive from the surface drag mechanism. The F_ψ terms represent the vorticity tendency terms due to the

shear advection and vertical advection mechanisms of baroclinic-barotropic interactions. The complete form of F_{ψ_0} is:

$$F_{\psi_0} = \frac{1}{a\cos\theta}\left[\frac{\partial}{\partial\lambda}(\bar{u}_1\nabla^2\psi_1' + u_1'\nabla^2\bar{\psi}_1) + \frac{\partial}{\partial\theta}(\cos\theta\bar{v}_1\nabla^2\psi_1' + \cos\theta v_1'\nabla^2\bar{\psi}_1)\right]$$

$$= \frac{1}{a\cos\theta}\left\{\begin{array}{l}\nabla^2\psi_1'\left[\frac{\partial\bar{u}_1}{\partial\lambda} + \frac{\partial}{\partial\theta}(\cos\theta\bar{v}_1)\right] + \nabla^2\bar{\psi}_1\left[\frac{\partial u_1'}{\partial\lambda} + \frac{\partial}{\partial\theta}(\cos\theta v_1')\right] \\ + \left[\bar{u}_1\frac{\partial\nabla^2\psi_1'}{\partial\lambda} + \bar{v}_1\frac{\partial}{\partial\theta}(\cos\theta\nabla^2\psi_1')\right] + \left[u_1'\frac{\partial\nabla^2\bar{\psi}_1}{\partial\lambda} + v_1'\frac{\partial}{\partial\theta}(\cos\theta\nabla^2\bar{\psi}_1)\right]\end{array}\right\} \quad (6)$$

The first term in the r.h.s. of (6) represents the vertical advection of anomalous baroclinic vorticity via background vertical wind. The second term represents the vertical advection of background baroclinic vorticity via anomalous vertical wind. The third term represents the zonal and meridional advection of anomalous baroclinic vorticity via background zonal and meridional shear. The fourth term represents the zonal and meridional advection of background baroclinic vorticity via anomalous zonal and meridional shear.

The thermodynamic equation is given by:

$$\gamma\phi_1 + c_g^2\nabla^2\chi_1 = -Q \quad (7)$$

where γ is the thermal damping coefficient, ϕ_1 is the baroclinic geopotential, c_g is the internal gravity wave speed, χ_1 is the baroclinic divergence and Q is the diabatic heating rate. Note that the simple model is explicitly steady state and linear and omits all moisture effects. The equations (4)-(7) together with a baroclinic divergence equation (not shown here) are in a closed form and are the governing equations solved in the simple model.

242 In our simple model experiments, we are able to activate and deactivate each forcing
243 mechanism—the surface drag, the vertical advection and the shear advection, and compare the
244 effects of each forcing with those in the QTCM results.

245 The numerical implementation of the three versions of the simple model covers the
246 domain from 90°S to 90°N over all longitudes, with a horizontal resolution of 4.5° latitude and
247 4.5° longitude.

248

249 *c. Methodology*

250 We concentrate on the period of June-August (JJA), during which the tropical heating
251 and precipitation anomalies develop to their maximum strength in the northern hemisphere
252 summer, including in the AWP region of interest here. In JJA, the subtropical jets are strong in
253 the southern (winter) hemisphere, which can favor the shear advection mechanism for
254 interhemispheric teleconnections (Wang et al. 2010). Accordingly, in both the QTCM and simple
255 model, the zonal mean of the barotropic and baroclinic wind fields are prescribed as the JJA
256 zonal means. The time advance of the zonal mean fields in the QTCM is, therefore, bypassed.
257 The prescribed velocities correspond to the streamfunction at the 250 and 750mb levels from the
258 monthly NCEP-NCAR reanalysis (Kalnay et al. 1996):

259 $$\bar{u}_0 = -\frac{\partial}{\partial y}\bar{\psi}_0^{ncep} = -\frac{\partial}{\partial y}[(\bar{\psi}_{250}^{ncep} + \bar{\psi}_{750}^{ncep})/2] \quad (8)$$

260 $$\bar{u}_1 = -\frac{\partial}{\partial y}\bar{\psi}_1^{ncep} = -\frac{\partial}{\partial y}[(\bar{\psi}_{250}^{ncep} - \bar{\psi}_{750}^{ncep})/2] \quad (9)$$

Further, in the QTCM we replace the zonal velocity that advects the temperature gradient by that corresponding to the zonal mean basic state velocity as in equations (8) and (9). This procedure removes the main source term for baroclinic instability, thus reducing weather variability. There are some trade-offs here. On the one hand, due to reduction in poleward fluxes, more moisture is available for precipitation in the subtropics, and interactions of the teleconnections with storm tracks are suppressed. On the other hand, the procedure has several advantages in view of our goals. These include (i) statistically significant signals are easy to detect in decadal runs, (ii) comparison to the simple model is facilitated, (iii) the basic state on which wave propagation occurs is strongly constrained towards observations, and (iv) interpretation in terms of stationary wave propagation is more straightforward. This should thus be viewed as an intermediate step between simple models and GCMS that would potentially include more complex effects such as interaction with baroclinic transients.

3. QTCM Experiments and Results

a. Atlantic Warm Pool (AWP) teleconnection experiments set up

In this experiment, we prescribe a Gaussian-shaped baroclinic heating anomaly as in Lee et al. (2009). The anomaly amplitude is 169.2W/m^2 (which is equivalent to 6mm/day of precipitation) at the center at (20°N, 70°W), and the zonal and meridional length scales are 5° latitude and 15° longitude (see Fig. 1a). The model is then run for ten years using monthly climatological SSTs (Reynolds and Smith 1994).

Figure 1b shows the precipitation response averaged over the June-August for ten years in response to the prescribed heating anomalies in this experiment. It can be seen that the latent

283 heat associated with the precipitation anomalies enhance the local prescribed heating anomalies
284 to a significant extent, and thus will enhance the teleconnection response in comparison to a
285 model with dry dynamics. The shape of the heating is also slightly modified from the prescribed.
286 We return to this moist feedback effect in section 3c.
287
288 *b. AWP teleconnections analysis*
289 The JJA mean baroclinic and barotropic streamfunctions anomalies are shown in Figs. 2a
290 and 2b. The baroclinic mode resembles the Gill–Matsuno-type response (Matsuno 1966; Gill
291 1980) and is equatorially trapped with most of the signal within equatorial deformation radius.
292 An important aspect is that the off-equatorial heating projects sufficiently on the Kelvin mode (to
293 the east of the heating) and the symmetric Rossby modes (to the west) that a substantial
294 baroclinic signal crosses the equator. The barotropic mode shows an interesting pattern.
295 Typically, a pure barotropic stationary Rossby wave propagating in a westerly region of the mid-
296 latitudes in an approximately barotropic basic state will approach a critical latitude where $\bar{u} = 0$
297 and thus will not propagate directly across the region of easterlies near equator. In our
298 experiments, however, the barotropic signal has a significant component in the southern
299 hemisphere. This is because the QTCM includes a full set of forcing sources of the barotropic
300 motions through baroclinic-barotropic interactions. As mentioned in section 2a, in the model's
301 barotropic component equation in QTCM, the three baroclinic forcing mechanisms—the shear
302 advection, surface drag, and vertical advection— actively generate barotropic wave trains in the
303 equatorial regions and within the southern hemisphere westerlies.
304 To explore the relative importance of the three mechanisms of interest in the QTCM
305 AWP experiment, we plot in Figs. 3a, 3b, 3c the amplitudes of the three terms in the r.h.s. of (3),

306 and in Figs. 4a, 4b, 4c their inverse Laplacians, i.e., the equivalent barotropic streamfunction
307 tendency terms. Shaded areas in Figs 3 and 4 represent values that are statistically significant
308 with a confidence level of 99% from a student's t-test. The shear advection term
309 $-curl_z(\langle V_1^2 \rangle \mathbf{v_1} \cdot \nabla \mathbf{v_1})'$ shows a large dipole in the tropics (Fig. 3a and 4a), roughly coincident
310 with where the baroclinic signal is strong. The southwest to northeast angle reflects the
311 corresponding tilt seen in Fig. 2 close to the zero contour of ψ_1 where the strong gradient in ψ_1
312 indicates strong baroclinic wind anomalies. Thus the region of strong shear forcing reflects the
313 heating-forced baroclinic anomalies which, while equatorially trapped, are able to propagate into
314 the southern hemisphere where they can excite barotropic waves.

315 The magnitude of the surface drag term $-curl_z(\varepsilon_0 \mathbf{v}_0 + \varepsilon_{10} \mathbf{v}_1)'$ in Fig. 3b is not locally as
316 large as that of the shear advection term (Fig. 3a) and vertical advection term (Fig. 3c), but its
317 inverse Laplacian (Fig. 4b) shows large values around the heat source with amplitudes
318 comparable with the vertical advection term. The geographical spread of the surface drag forcing
319 is broader in both hemispheres than the two other mechanisms. Note that Figs. 3b and 4b show
320 the net effect of surface drag mechanism, i.e., the amplitude of the baroclinic forcing
321 $-curl_z(\varepsilon_{10} \mathbf{v}_1')$ after compensation by linear damping $-curl_z(\varepsilon_0 \mathbf{v}_0')$. Also note that the sign of the
322 coefficient of transfer by surface stress between baroclinic and barotropic wind components ε_{10} is
323 negative in order that all the turbulence terms have the same form (refer to the appendix for more
324 detail). For a rough estimate of this compensation, comparing the amplitudes of $-\varepsilon_{10}\psi_1$ (where
325 $\varepsilon_{10} = (-28\text{day})^{-1}$ and ψ_1 can be approximated from the values in Fig. 2a) and $-\varepsilon_0\psi_0$ (where
326 $\varepsilon_0 = (5.6\text{day})^{-1}$ and ψ_0 can be approximated from the values in Fig. 2b), indicates that the
327 compensation effect of the linear damping can be as large as 50% of the baroclinic forcing. This

328 estimate is confirmed by Fig. 3d, showing only the baroclinic forcing component of the surface
329 drag $-curl_z(\varepsilon_{10}\mathbf{v}_1')$. As expected, this component is roughly twice as large locally as the total
330 surface drag term (Fig. 3b). We can also see that the surface drag component has a significant
331 contribution in the southern hemisphere. Thus the baroclinic forcing from the surface drag term
332 can potentially exert a substantial impact on the generation and propagation of barotropic Rossby
333 waves, especially in the southern hemisphere corresponding to the ψ_1 response there.

334 Finally, the vertical advection term $-curl_z(\langle V_1^2 \rangle (\nabla \cdot \mathbf{v_1})\mathbf{v_1})'$ (Figs. 3c and 4c) shows a
335 localized forcing around the heat source where the vertical velocity is large (also see Fig. 1b for
336 large local precipitation anomaly there). Note that some degree of compensation can occur with
337 the surface drag term in regions of upward vertical motion where the vertical velocity term
338 contribution $-\langle V_1^2 \rangle (\nabla \cdot \bar{\mathbf{v}}_1) curl_z \mathbf{v}_1'$ has opposite sign but similar form to $-curl_z(\varepsilon_{10}\mathbf{v}_1')$. Far from the
339 heat source, in certain regions of the Pacific and Indian Ocean, the vertical velocity term can still
340 have fairly substantial contributions corresponding to the remote precipitation anomalies in those
341 regions. The strong vertical advection forcing locally around the heat source (Fig. 3c) and the
342 remote signals in the southern hemisphere imply that this mechanism has a substantial role in the
343 interhemispheric teleconnections, and should not be neglected.
344
345 *c. Moist feedback*

346 The precipitation response in the QTCM AWP experiments is shown in Fig. 1b. There is
347 clear evidence that moist processes enhance the teleconnection process. First, moist feedback
348 enhances the prescribed anomalous heat source locally by approximately 6mm/day in this
349 experiment, which is as large as the prescribed heat source. Second, the shape of the precipitation
350 anomaly is stretched southwestward into eastern Pacific region. A similar feature is apparent in

351 the GCM AWP experiments in Wang et al. (2007, 2008). This precipitation anomaly is the result
352 of the Atlantic Warm Pool-induced subtropical Rossby waves propagating westward and
353 interacting with the Intertropical Convergence Zone (ITCZ) in the eastern Pacific. The impact of
354 this convective heating anomaly in the eastern Pacific is further analyzed in section 3d. Third,
355 this elongated shape, and the compensating subsidence north of the precipitation anomaly are
356 consistent with the mechanism described in Chou and Neelin (2003) as the result of the
357 interaction between baroclinic Rossby wave dynamics and convective heating. The subsidence
358 may modestly impact the teleconnection patterns north of the heating anomaly by reducing the
359 baroclinic signal extent and by contributing to vertical advection. Finally, as the flow anomalies
360 produced by the teleconnections interact with moist processes remotely, e.g., advecting the basic
361 state moisture gradient, they can induce remote precipitation anomalies that can contribute to the
362 baroclinic-barotropic interaction. For instance, Fig. 1b shows precipitation anomalies in the
363 equatorial Western Pacific and in the subtropical Southeastern Pacific. The latter corresponds to
364 a significant contribution to the vertical advection forcing term in Figs. 3c and 4c in the southern
365 hemisphere.
366
367 *d. The impact of the response in the eastern Pacific ITCZ region*
368 As mentioned in section 3c, the moist feedback on the teleconnections leads to an
369 elongation of the anomalous heat source in the AWP region into the eastern Pacific ITCZ region.
370 This elongation is also seen in the AGCM experiments of Want et al. (2007, 2008). Here, we
371 investigate quantitatively the influence of this additional heating in the ITCZ region on the AWP
372 teleconnections into the southern hemisphere. We prescribe a similar Gaussian-shaped baroclinic
373 heating anomaly with the same amplitude as in the one above the AWP, but with the center at

374 (15°N, 95°W), and scales of 3.0° latitude and 7.5° longitude. The model is then run for ten years
375 using monthly climatological SSTs (Reynolds and Smith 1994).

376 Fig. 5 shows the barotropic streamfunction response to the heating prescribed in the
377 eastern Pacific region. A comparison between this and Fig. 2b, reveals an overlap of the positive
378 and negative phases of the response induced by the two different heating regions, and confirms
379 that the induced eastern Pacific heating provides a positive feedback to the original AWP
380 heating. We have also tested the result's sensitivity to the extension of the elongation, and found
381 that the model response to a further elongation into the eastern Pacific as that in the AGCM
382 experiments of Want et al. (2007, 2008) has an extremely similar pattern (not shown).

383

384 e. *Sensitivity of the teleconnection pattern to longitudinal location of heating anomaly*

385 To explore the dependence of the teleconnection response to the heating location in
386 longitude, we perform a supplementary experiment in which the heating source is placed in the
387 central Pacific at a location 90° in longitude west of the AWP (see Fig. 6a). The precipitation
388 anomalies in this experiment are shown in Fig. 6b, while the baroclinic and barotropic
389 streamfunctions response are shown in Figs. 7a and 7b, respectively. The zonally asymmetric
390 basic state in the model can affect wave propagation, but some of the most obvious differences
391 arise in the moist response to the source. The precipitation anomalies do not show a similar
392 elongation as those in the AWP experiment (Fig. 1b), which leads to smaller zonal wavelengths
393 in the baroclinic and hence in the barotropic response (Fig. 7b). Based on the WKB theory for
394 stationary barotropic Rossby wave propagation in latitudinally varying flow, the local meridional
395 wave number $l(y)$ is given by $l(y) = \pm(\hat{\beta}\overline{u}_m^{-1} - k^2)^{1/2}$, where k is the zonal wave number, $\hat{\beta}$
396 and $\overline{u}_m$ are basic state vorticity and zonal mean flow variables defined in Mercator coordinates

equivalent to the form on a beta-plane with spherical effects incorporated (Hoskins and Karoly 1981). The smaller zonal wavelengths (larger zonal wave number k) mean a lower turning latitude because the local meridional wave number for stationary barotropic Rossby waves goes to zero at smaller values of $\hat{\beta}\overline{u}_m^{-1}$. Thus the wave arc in the northern hemisphere is more zonal. In the southern hemisphere, the barotropic responses in both the AWP and central Pacific experiments (Figs. 2b and 7b) are qualitatively similar, but the latter one has weaker magnitudes. This is partly due to the small baroclinic response in the southern hemisphere (Fig. 7a), and to the absence of the vertical advection forcing sources in the southern Pacific (Figs. 3c and 4c).

4. Simple Model experiments

In the simple model, an identical Gaussian-shaped heating anomaly is prescribed in the AWP region with a diabatic heating rate of $2.5\times10^{-2}\,\mathrm{W\,kg^{-1}}$, which is equivalent to $2.15\ \mathrm{K\,day^{-1}}$ at 500mb. For the simple vertical structure of this model (linear within each layer), this would be roughly equivalent to $127.6\ \mathrm{W\,m^{-2}}$ using 500mb layer depth. This heating anomaly is the only heat source since there is no moist feedback in the model. Recall from section 2, that the model is linearized about the basic state from JJA NCEP-NCAR reanalysis streamfunction averaged zonally around the globe. Other model parameters used in the present study are the same as those in Lee et al. (2009) with the following exceptions. The barotropic and baroclinic linear damping coefficient is set to $(3.5\mathrm{day})^{-1}$ for compatibility with the QTCM; and the barotropic horizontal mixing coefficient is set to $2.5\times10^{5}\,\mathrm{m^2s^{-1}}$ following Wang et al (2010). Altering these damping coefficients affects the rate at which the barotropic wave decays.

418 Figures 8a shows the barotropic streamfunctions response in the model with shear
419 advection mechanism, and Fig. 8b shows the corresponding values with both shear advection and
420 surface drag mechanisms included (Note that the latitude coverage is adjusted to 78.75°S to
421 78.75°N in order to compare with the QTCM results). Addition of the surface drag mechanism
422 results in a strong amplification and extension of the barotropic response in the southern
423 hemisphere. This supports the finding in the QTCM experiments that the surface drag
424 mechanism is potentially very effective in forcing the barotropic response globally, especially in
425 spreading the cross-equatorial barotropic signals.

426 Figure 8c shows the barotropic streamfunction response of the model experiment with
427 both the shear advection and the vertical advection mechanisms. Comparing with Fig. 8a, as in
428 the QTCM experiment, the vertical advection amplifies the barotropic response locally around
429 the heating area, and spreads the barotropic signals into the southern hemisphere, although the
430 impact is moderate compared to the surface drag mechanism.

431

432 5. Summary and discussion

433 We have investigated the mechanisms that control the interhemispheric
434 teleconnections from tropical heat sources. Our approach is based on the analysis of the response
435 to idealized distributions of tropical heating sources in experiments in QTCM and in a simple
436 steady-state, damped, linear stationary wave model. We concentrated primarily in the Atlantic
437 Warm Pool region to prescribe the heating because it has been identified as significant in setting
438 up interhemispheric influence in previous studies (e.g., Wang et al. 2010). The direct baroclinic
439 response to this tropical heating is approximately a Gill–Matsuno-type response (Matsuno 1966;

Gill 1980), which is equatorially trapped. The teleconnections to mid and high latitudes are dominated by barotropic mode. The baroclinic to barotropic pathway is complex involving the basic state shear with all its spatial dependence, as well as the basic state vertical velocity and surface drag. In absence of basic state shear and vertical velocity and of surface drag, baroclinic and barotropic components are decoupled. This makes the recent literature examining the role of these interaction terms as a driver for barotropic motions from heat forced baroclinic motions (e.g., Neelin and Zeng 2000, Majda and Biello 2003, Lee et al. 2009) appear very different from the earlier literature that assumed upper-level divergence and related terms could be viewed as a driver (e.g., Sardeshmukh and Hoskins 1988, Held and Kang 1987), often summarized as a vorticity source term (the "Rossby wave source") for a single-level barotropic equation. Here we diagnose the interaction terms as a consistent vorticity source for the barotropic mode in a primitive equation model that has an explicit vertical mode decomposition. In addition to explicit computation of the interaction terms as in earlier theoretical studies, the study retains a complex three-dimensional basic state and moist processes for a quantitative examination.

The interaction-term framework results in some very substantial differences in the way one views the teleconnections generated by anomalous heating. First, it should be noted that upper-level divergence in the baroclinic mode does not necessarily drive a response in the barotropic mode, as is commonly assumed, unless appropriate conditions such as basic state shear occur in the regions of descent. Furthermore, for interhemispheric teleconnections or tropical to mid-latitude teleconnections, the first leg of the teleconnection occurs in the baroclinic mode. Equatorially trapped baroclinic waves can be responsible for most of the propagation within regions where low-frequency barotropic modes are evanescent, including across the equator. Diagnosis of interaction terms as a forcing in the barotropic equation in the QTCM

463 results then allows us to identify the relative importance of each mechanism in exciting the
464 barotropic mode: the shear advection mechanism, the surface drag mechanism and the vertical
465 advection mechanism. In these results, the Rossby wave source in the barotropic equation due to
466 shear advection roughly coincides with the baroclinic signal in the tropics and subtropics, and
467 thus can be effective in contributing to the southern hemisphere response to an Atlantic Warm
468 Pool heat source. The barotropic Rossby wave source due to surface drag is more broadly
469 spatially spread, essentially reflecting the contribution of the baroclinic mode to low-level wind,
470 and has large enough magnitude to provide a substantial forcing mechanism for interhemispheric
471 teleconnections. Last, the barotropic Rossby wave source due to vertical advection is significant
472 in locations where the climatological vertical velocity and vertical shear are both large. These
473 mechanisms were further examined by modifying the simple model to include the surface drag
474 and vertical advection one by one, and by comparing their effects with the shear advection
475 mechanism. The results from the simple model provide support to the interpretation of QTCM
476 results.

477 The QTCM results also allowed for an assessment of effects that moist feedbacks can
478 have in such interhemispheric teleconnections. Moist processes strengthen the initial heating
479 locally. In the Atlantic Warm Pool experiment, the region of anomalous heating is extended
480 westward by the induced precipitation anomalies in the Eastern Pacific ITCZ region. This
481 amplifies the original teleconnection response, as shown if these anomalies are applied
482 separately. Such an effect depends on the regional basic state: it does not occur for a similar
483 initial anomaly applied in the central Pacific. Additional moist feedbacks can occur remotely. In
484 the Atlantic warm pool experiment, induced precipitation anomalies are obtained in both the
485 equatorial Western Pacific and the subtropical Eastern Pacific. The latter contribute to the

vertical advection forcing of barotropic motions in the southern hemisphere. The total moist feedback on the teleconnection process is thus able to alter significantly the teleconnection response to tropical heating.

Acknowledgments

We thank Joyce Meyerson and Katrina Hales in their help and support in running the QTCM. We also thank Joyce Meyerson for her graphical work for this paper. This work was supported by National Science Foundation Grant AGS-1102838 and AGS-1041477.

APPENDIX

QTCM equations

QTCM is a nonlinear tropical circulation model that makes use of constraints from a particular QE convective scheme, the Betts-Miller scheme, but does not assume that convective QE has to hold. To achieve this, temperature, velocity and moisture are expanded in terms of a truncated series of basis functions in the vertical:

$$T = T_r(p) + \sum_{k=1}^{K} a_k(p) T_k(x,y,t) \qquad \text{(A1)}$$

$$\mathbf{v} = \sum_{k=0}^{L} V_k(p) \mathbf{v}_k(x,y,t) \qquad \text{(A2)}$$

$$q = q_r(p) + \sum_{k=1}^{K} b_k(p) q_k(x,y,t) \qquad \text{(A3)}$$

The model simply takes analytical solutions that hold approximately under QE conditions and employs them as leading basis functions to represent the vertical structure of the flow.

For the standard version of QTCM1, a single deep convective mode is retained in the vertical thermodynamic structure (i.e., $T = T_r(p) + a_1(p)T_1(x,y,t)$) with two components (barotropic $V_0(p)$ and baroclinic $V_1(p)$) in the vertical structure of velocity. Discretization of the moisture equation is largely independent. The model simply chooses a truncation for the moisture equation to have a similar level of complexity as for the temperature equation.

Using V_0 and V_1 as the basis functions, the momentum equations are projected onto these (i.e., taking the inner product of the momentum equation with V_0 and V_1 respectively) to obtain the prognostic equations for barotropic wind component and baroclinic wind component:

$$\partial_t \zeta_0 + curl_z(\mathcal{D}_{V0}(\mathbf{v_0}, \mathbf{v_1})) + \beta v_0 = -curl_z(\varepsilon_0 \mathbf{v_0}) - curl_z(\varepsilon_{10} \mathbf{v_1}) \quad \text{(A4)}$$

$$\partial_t \mathbf{v}_1 + \mathcal{D}_{V1}(\mathbf{v_0}, \mathbf{v_1}) + f\mathbf{k} \times \mathbf{v}_1 = -\kappa \nabla T_1 - \varepsilon_1 \mathbf{v}_1 - \varepsilon_{01} \mathbf{v}_0 \quad \text{(A5)}$$

where the advection-diffusion operators are given by:

$$\mathcal{D}_{V0}(\mathbf{v_0}, \mathbf{v_1}) = \mathbf{v_0} \cdot \nabla \mathbf{v_0} + \left\langle V_1^2 \right\rangle \mathbf{v_1} \cdot \nabla \mathbf{v_1} + \left\langle V_1^2 \right\rangle (\nabla \cdot \mathbf{v_1}) \mathbf{v_1} - K_H \nabla^2 \mathbf{v_0} \quad \text{(A6)}$$

$$\mathcal{D}_{V1}(\mathbf{v_0}, \mathbf{v_1}) = \mathbf{v_0} \cdot \nabla \mathbf{v}_1 + \frac{\left\langle V_1^3 \right\rangle}{\left\langle V_1^2 \right\rangle} \mathbf{v_1} \cdot \nabla \mathbf{v_1} + \mathbf{v}_1 \cdot \nabla \mathbf{v_0} - (\left\langle V_1 \Omega_1 \partial_p V_1 \right\rangle / \left\langle V_1^2 \right\rangle)(\nabla \cdot \mathbf{v_1}) \mathbf{v_1} - K_H \nabla^2 \mathbf{v}_1 \quad \text{(A7)}$$

vertical averages over the troposphere are defined as:

$$\hat{X} = \langle X \rangle = p_T^{-1} \int_{p_{rt}}^{p_{rs}} X dp \quad \text{(A8)}$$

and $\Omega_1(p)$ represents the vertical structure of vertical velocity from the baroclinic wind. Because vertical velocity is diagnostic in the primitive equations, solving the continuity equation gives:

$$\omega_1(x,y,p,t) = -\Omega_1(p)\nabla\cdot\mathbf{v}_1(x,y,t) \quad \text{(A9)}$$

$$\text{and} \quad \Omega_1(p) = -\int_p^{p_s} V_1(p)dp \quad \text{(A10)}$$

Two of the terms arising from vertical transfer of momentum to surface stress by parameterized subgrid-scale turbulence in the barotropic equation are defined as:

$$\varepsilon_0 = (g/p_T)\rho_a C_D V_s \quad \text{(A11)}$$

$$\varepsilon_{10} = (g/p_T)\rho_a C_D V_s V_{1s} \quad \text{(A12)}$$

where V_s is calculated as $\sqrt{u_s^2 + v_s^2 + V_{s\min}^2}$, and V_{1s} is value of the baroclinic basis function V_1 at surface. The surface drag coefficient C_D changes according to land surface type. The sign of ε_0 and ε_{10} are set as opposite in the model in order that the two surface drag terms has the same form.

Vertically integrating the temperature and moisture equations from the standard nonlinear primitive equations, with vertical velocity and velocity truncated at V_1 yields:

$$\hat{a}_1(\partial_t + \mathcal{D}_{T1})T_1 + M_{S1}\nabla\cdot\mathbf{v}_1 = \langle Q_c\rangle + (g/p_T)\times(-R_t^{\uparrow} - R_s^{\downarrow} + R_s^{\uparrow} + S_t - S_s + H) \quad \text{(A13)}$$

$$\hat{b}_1(\partial_t + \mathcal{D}_{q1})q_1 + M_{q1}\nabla\cdot\mathbf{v}_1 = \langle Q_q\rangle + (g/p_T)E \quad \text{(A14)}$$

where the advection-diffusion operators are, respectively:

$$\mathcal{D}_{T1} = \mathbf{v}_0\cdot\nabla + \hat{a}_1^{-1}\langle a_1 V_1\rangle\mathbf{v}_1\cdot\nabla - K_H\nabla^2 \quad \text{(A15)}$$

$$\mathcal{D}_{q1} = \mathbf{v}_0\cdot\nabla + \hat{b}_1^{-1}\langle b_1 V_1\rangle\mathbf{v}_1\cdot\nabla - K_H\nabla^2 \quad \text{(A16)}$$

and the dry static stability M_{S1} and the gross moisture stratification M_{q1} are given by, respectively:

$$M_{S1} = p_T^{-1} \int_{p_{rt}}^{p_{rs}} \Omega_1(-\partial_p s) dp \quad \text{(A17)}$$

$$M_{q1} = p_T^{-1} \int_{p_{rt}}^{p_{rs}} \Omega_1(-\partial_p q) dp \quad \text{(A18)}$$

where $s = T + \phi$ is the dry static energy, with ϕ the geopotential. The moist convective parameterization projects the Betts – Miller scheme onto the basis functions of temperature and moisture, resulting in:

$$\langle Q_c \rangle = -\langle Q_q \rangle = \varepsilon_c^* (q_1 - T_1) \quad \text{(A19)}$$

where $\varepsilon_c^* \equiv \hat{a}_1 \hat{b}_1 (\hat{a}_1 + \hat{b}_1)^{-1} \varepsilon_c$ and $\varepsilon_c = \tau_c^{-1} \mathcal{H}(C_1)$, with τ_c the convective adjustment time, $\mathcal{H}(C_1)$ a Heaviside function that represents the dependence of convection on conditional instability in the column, and C_1 a measure of CAPE for this model. Detailed treatment and parameterization of other terms on the right hand side of the temperature and moisture equations can be found in Neelin and Zeng (2000).

References

Barnston, A. G., and Coauthors, 1999: NCEP forecasts of the El Nino of 1997-98 and its US impacts. *B Am Meteorol Soc*, **80,** 1829-1852.

Biello, J. A., and A. J. Majda, 2004a: Boundary layer dissipation and the nonlinear interaction of equatorial baroclinic and barotropic Rossby waves. *Geophys Astro Fluid*, **98,** 85-127.

——, 2004b: The effect of meridional and vertical shear on the interaction of equatorial baroclinic and barotropic Rossby waves. *Stud Appl Math*, **112,** 341-390.

Chou, C., and J. D. Neelin, 2003: Mechanisms limiting the northward extent of the northern summer monsoons over North America, Asia, and Africa. *J Climate*, **16,** 406-425.

DeWeaver, E., and S. Nigam, 2004: On the Forcing of ENSO Teleconnections by Anomalous Heating and Cooling. *J Climate*, **17,** 3225-3235.

Gill, A. E., 1980: Some Simple Solutions for Heat-Induced Tropical Circulation. *Q J Roy Meteor Soc*, **106,** 447-462.

Goddard, L., and N. E. Graham, 1999: Importance of the Indian Ocean for simulating rainfall anomalies over eastern and southern Africa. *J Geophys Res-Atmos*, **104,** 19099-19116.

Held, I. M., and I. S. Kang, 1987: Barotropic Models of the Extratropical Response to El-Nino. *J Atmos Sci*, **44,** 3576-3586.

Held, I. M., R. L. Panetta, and R. T. Pierrehumbert, 1985: Stationary External Rossby Waves in Vertical Shear. *J Atmos Sci*, **42,** 865-883.

Held, I. M., S. W. Lyons, and S. Nigam, 1989: Transients and the Extratropical Response to El-Nino. *J Atmos Sci*, **46,** 163-174.

Hoerling, M. P., and M. F. Ting, 1994: Organization of Extratropical Transients during El-Nino. *J Climate*, **7,** 745-766.

576 Horel, J. D., and J. M. Wallace, 1981: Planetary-Scale Atmospheric Phenomena Associated with
577 the Southern Oscillation. *Mon Weather Rev*, **109,** 813-829.
578 Hoskins, B. J., and D. J. Karoly, 1981: The Steady Linear Response of a Spherical Atmosphere
579 to Thermal and Orographic Forcing. *J Atmos Sci*, **38,** 1179-1196.
580 Kalnay, E., and Coauthors, 1996: The NCEP/NCAR 40-year reanalysis project. *B Am Meteorol*
581 *Soc*, **77,** 437-471.
582 Kumar, A., and M. P. Hoerling, 1998: Specification of regional sea surface temperatures in
583 atmospheric general circulation model simulations. *J Geophys Res-Atmos*, **103,** 8901-8907.
584 Latif, M., D. Dommenget, M. Dima, and A. Grotzner, 1999: The role of Indian Ocean sea
585 surface temperature in forcing east African rainfall anomalies during December-January
586 1997/98. *J Climate*, **12,** 3497-3504.
587 Lau, N. C., 1985: Modeling the Seasonal Dependence of the Atmospheric Response to Observed
588 El-Ninos in 1962-76. *Mon Weather Rev*, **113,** 1970-1996.
589 Lee, S. K., C. Z. Wang, and B. E. Mapes, 2009: A Simple Atmospheric Model of the Local and
590 Teleconnection Responses to Tropical Heating Anomalies. *J Climate*, **22,** 272-284.
591 Lin, J. W. B., and J. D. Neelin, 2000: Influence of a stochastic moist convective parameterization
592 on tropical climate variability. *Geophys Res Lett*, **27,** 3691-3694.
593 ——, 2002: Considerations for stochastic convective parameterization. *J Atmos Sci*, **59,** 959-975.
594 Lin, J. W. B., J. D. Neelin, and N. Zeng, 2000: Maintenance of tropical intraseasonal variability:
595 Impact of evaporation-wind feedback and midlatitude storms. *J Atmos Sci*, **57,** 2793-2823.
596 Majda, A. J., and J. A. Biello, 2003: The nonlinear interaction of barotropic and equatorial
597 baroclinic Rossby waves. *J Atmos Sci*, **60,** 1809-1821.

598 Matsuno, T., 1966: Quasi-geostrophicmotions in the equatorial area. *J. Meteor. Soc. Japan*, **44,**
599 25–43.
600 Mechoso, C. R., A. Kitoh, S. Moorthi, and A. Arakawa, 1987: Numerical Simulations of the
601 Atmospheric Response to a Sea-Surface Temperature Anomaly over the Equatorial Eastern
602 Pacific-Ocean. *Mon Weather Rev*, **115,** 2936-2956.
603 Neelin, J. D., and N. Zeng, 2000: A quasi-equilibrium tropical circulation model - Formulation. *J*
604 *Atmos Sci*, **57,** 1741-1766.
605 Neelin, J. D., and H. Su, 2005: Moist teleconnection mechanisms for the tropical South
606 American and Atlantic sector. *J Climate*, **18,** 3928-3950.
607 Reynolds, R. W., and T. M. Smith, 1994: Improved Global Sea-Surface Temperature Analyses
608 Using Optimum Interpolation. *J Climate*, **7,** 929-948.
609 Ropelewski, C. F., and M. S. Halpert, 1987: Global and Regional Scale Precipitation Patterns
610 Associated with the El-Nino Southern Oscillation. *Mon Weather Rev*, **115,** 1606-1626.
611 Salby, M. L., and R. R. Garcia, 1987: Vacillations Induced by Interference of Stationary and
612 Traveling Planetary-Waves. *J Atmos Sci*, **44,** 2679-2711.
613 Saravanan, R., and P. Chang, 2000: Interaction between tropical Atlantic variability and El Nino-
614 Southern Oscillation. *J Climate*, **13,** 2177-2194.
615 Sardeshmukh, P. D., and B. J. Hoskins, 1988: The Generation of Global Rotational Flow by
616 Steady Idealized Tropical Divergence. *J Atmos Sci*, **45,** 1228-1251.
617 Simmons, A. J., 1982: The Forcing of Stationary Wave Motion by Tropical Diabatic Heating. *Q*
618 *J Roy Meteor Soc*, **108,** 503-534.
619 Simmons, A. J., J. M. Wallace, and G. W. Branstator, 1983: Barotropic Wave-Propagation and
620 Instability, and Atmospheric Teleconnection Patterns. *J Atmos Sci*, **40,** 1363-1392.

621 Su, H., and J. D. Neelin, 2002: Teleconnection mechanisms for tropical Pacific descent
622 anomalies during El Nino. *J Atmos Sci*, **59,** 2694-2712.
623 Ting, M. F., and I. M. Held, 1990: The Stationary Wave Response to a Tropical SST Anomaly in
624 an Idealized GCM. *J Atmos Sci*, **47,** 2546-2566.
625 Trenberth, K. E., G. W. Branstator, D. Karoly, A. Kumar, N. C. Lau, and C. Ropelewski, 1998:
626 Progress during TOGA in understanding and modeling global teleconnections associated with
627 tropical sea surface temperatures. *J Geophys Res-Oceans*, **103,** 14291-14324.
628 Wallace, J. M., E. M. Rasmusson, T. P. Mitchell, V. E. Kousky, E. S. Sarachik, and H. von
629 Storch, 1998: The structure and evolution of ENSO-related climate variability in the tropical
630 Pacific: Lessons from TOGA. *J Geophys Res-Oceans*, **103,** 14241-14259.
631 Wang, C. Z., S. K. Lee, and D. B. Enfield, 2007: Impact of the Atlantic warm pool on the
632 summer climate of the Western Hemisphere. *J Climate*, **20,** 5021-5040.
633 ——, 2008: Climate response to anomalously large and small Atlantic warm pools during the
634 summer. *J Climate*, **21,** 2437-2450.
635 Wang, C. Z., S. K. Lee, and C. R. Mechoso, 2010: Interhemispheric Influence of the Atlantic
636 Warm Pool on the Southeastern Pacific. *J Climate*, **23,** 404-418.
637 Webster, P. J., 1972: Response of Tropical Atmosphere to Local, Steady Forcing. *Mon Weather*
638 *Rev*, **100,** 518-&.
639 Zeng, N., J. D. Neelin, and C. Chou, 2000: A quasi-equilibrium tropical circulation model -
640 Implementation and simulation. *J Atmos Sci*, **57,** 1767-1796.

641

642

List of Figures

662 FIG. 5. The barotropic streamfunction anomalies in the Eastern Pacific experiment in QTCM.
663 Negative contour lines are dashed. The contour interval is 2 x 10^5 m^2 s^{-1}. The shaded area is the
664 heating prescribed in the eastern Pacific, with interval 1mm/day.

665 FIG. 6. (a) As in Fig. 1a, except shifting the heat source 90° in longitude to the central Pacific
666 region. (b) Precipitation anomalies in the central Pacific experiment in the QTCM. Negative
667 contour lines are dashed. The contour intervals are both 1mm/day.

668 FIG. 7. The baroclinic streamfunction anomalies (a) and barotropic streamfunction anomalies (b)
669 in the central Pacific experiment in QTCM. Negative contour lines are dashed. The contour
670 intervals are 2 x 10^6 m^2 s^{-1} in (a) and 2 x 10^5 m^2 s^{-1} in (b).

671 FIG. 8. The barotropic streamfunctions anomalies in the simple model AWP experiment (a) with
672 shear advection; (b) with shear advection and surface drag mechanisms; (c) with shear advection
673 and vertical advection mechanisms. Negative contour lines are dashed. The contour intervals are
674 2 x 10^5 m^2 s^{-1} in all three.

675

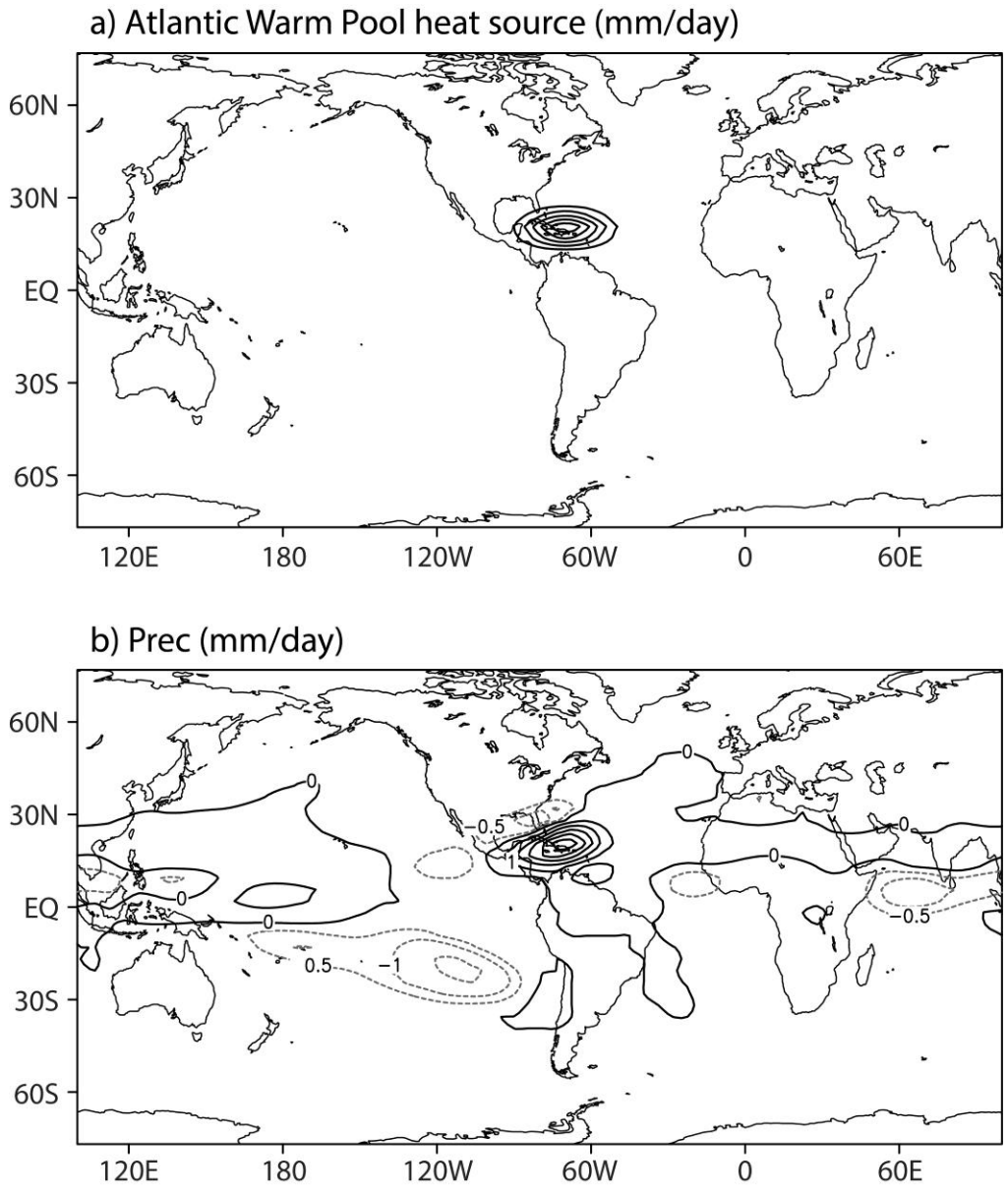

FIG. 1. (a) The Gaussian-shaped baroclinic heating anomaly prescribed in the Atlantic Warm Pool region in QTCM, the amplitude at the center (20°N, 70°W) is equivalent to 6mm/day of precipitation (i.e., 169.2W/m^2). (b) The precipitation anomalies in QTCM AWP experiment, negative contour lines are dashed. The contour intervals in both are 1mm/day (the 0.5mm/day precipitation contour is shown for easier recognition of the pattern).

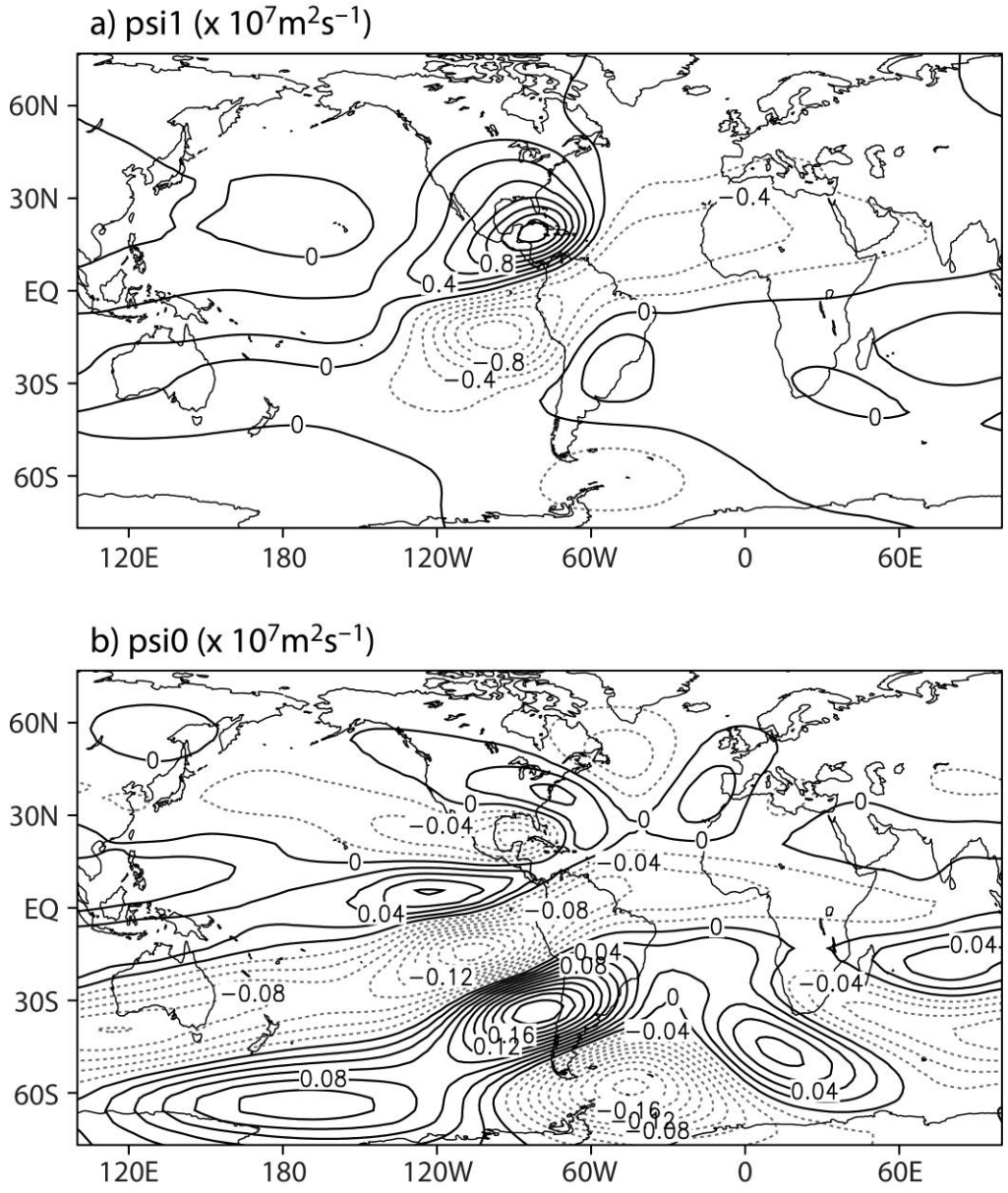

683

684 FIG. 2. The baroclinic streamfunction anomalies (a) and barotropic streamfunction anomalies (b)

685 in the AWP experiment in QTCM. Negative contour lines are dashed. The contour intervals are 2

686 x 10^6 m^2 s^{-1} in (a) and 2 x 10^5 m^2 s^{-1} in (b).

687

688

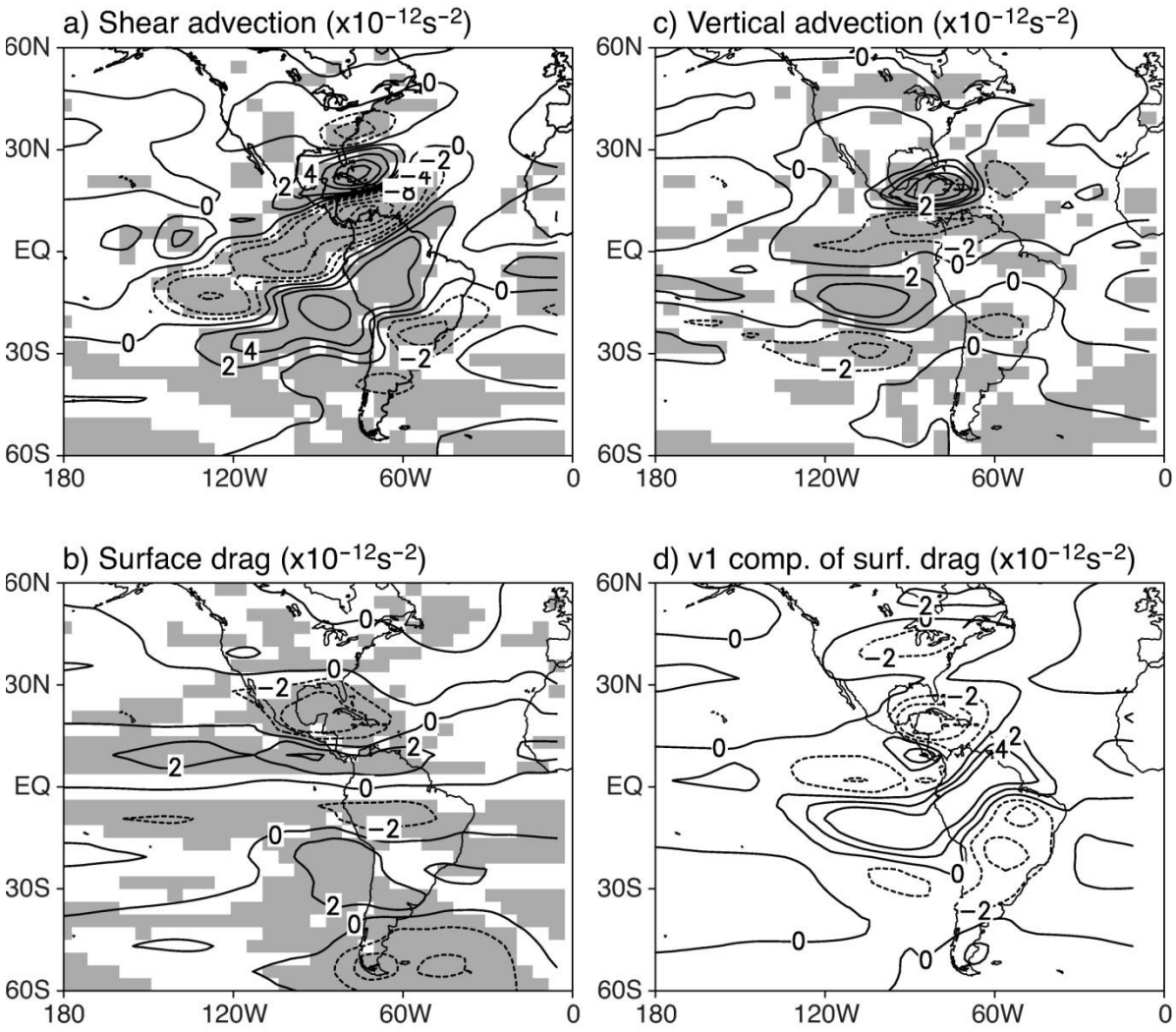

689

690 FIG. 3. The three forcing sources in the QTCM AWP experiment: (a) shear advection; (b)
691 surface drag; (c) vertical advection; and (d) v1 component of the surface drag (see text for
692 explanation). Negative contour lines are dashed. The contour intervals are $2x10^{-12}$ s^{-2} within
693 $\pm 4x10^{-12}$ s^{-2} and $4x10^{-12}$ s^{-2} outside $\pm 4x10^{-12}$ s^{-2} in all four panels. Shaded areas represent values
694 that are statistically significant with a confidence level of 99% from a student's t-test.

695

696

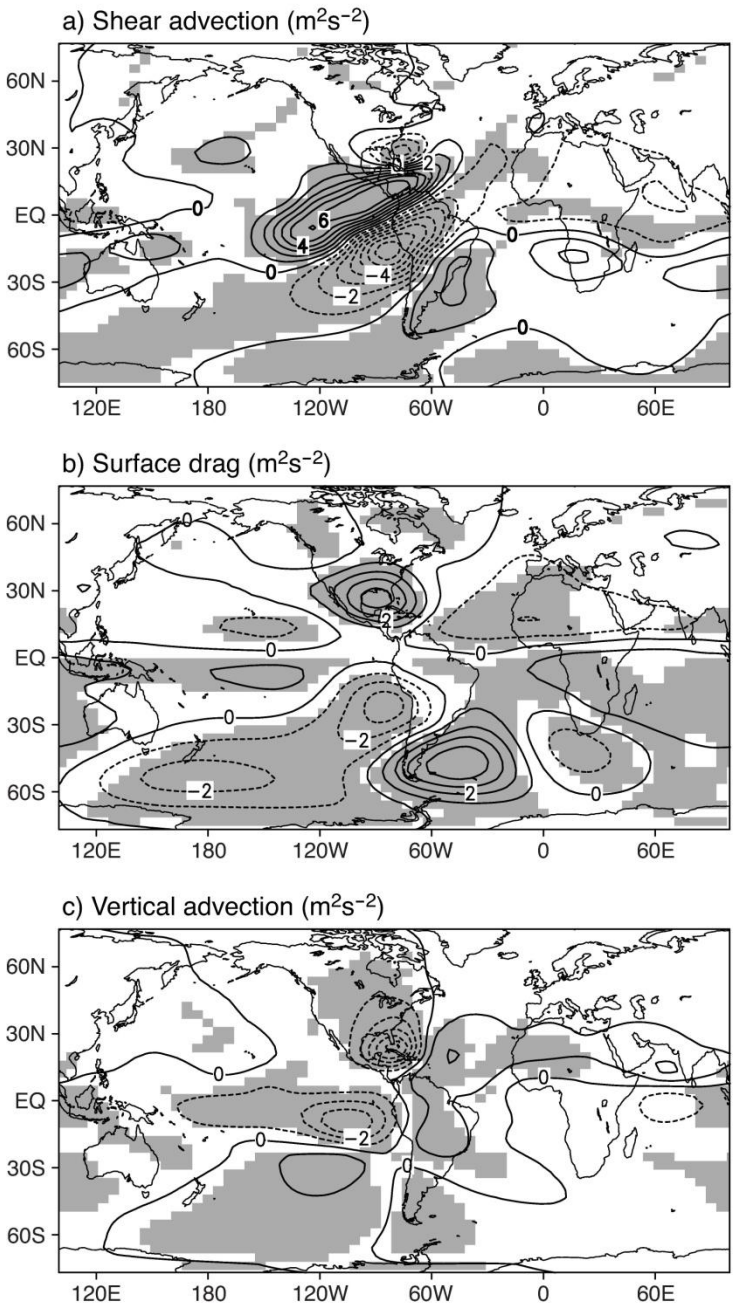

697

698 FIG. 4. The inverse Laplacian of the three forcing sources in the QTCM AWP experiment: (a)
699 shear advection; (b) surface drag; (c) vertical advection. Negative contour lines are dashed. The
700 contour intervals are 1 m^2 s^{-1} in all three. Shaded areas represent values that are statistically
701 significant with a confidence level of 99% from a student's t-test.

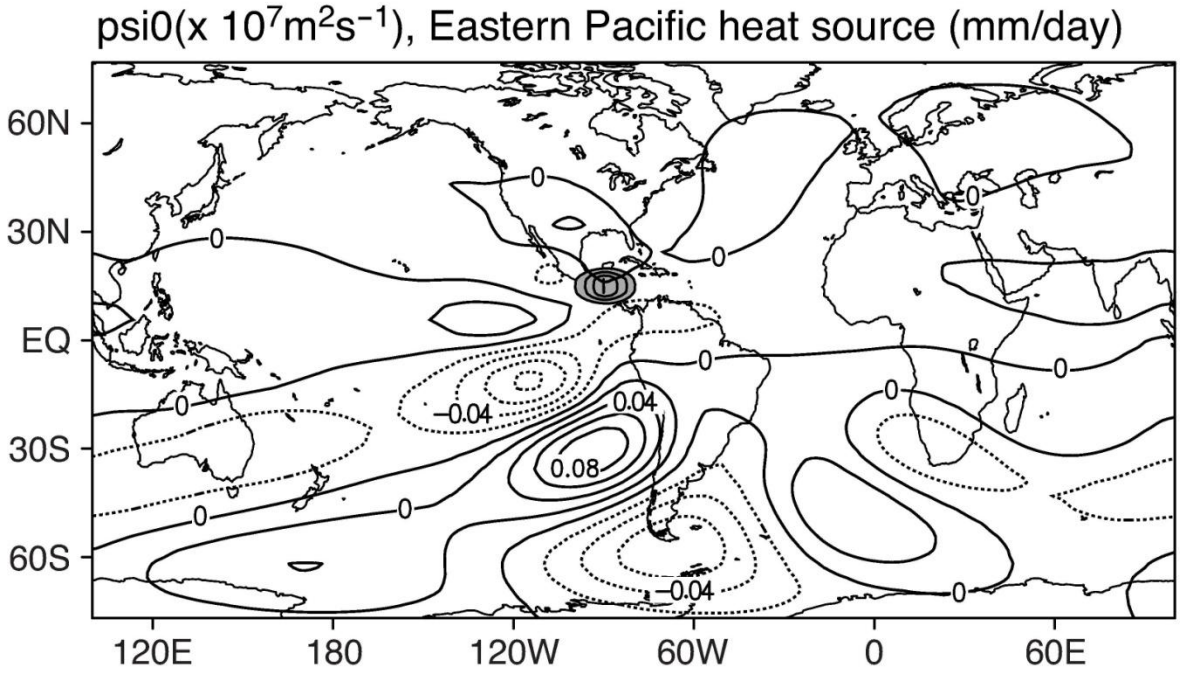

FIG. 5. The barotropic streamfunction anomalies in the Eastern Pacific experiment in QTCM. Negative contour lines are dashed. The contour interval is 2 x 10^5 m^2 s^{-1}. The shaded area indicates the heating prescribed in the eastern Pacific, with interval 1mm/day.

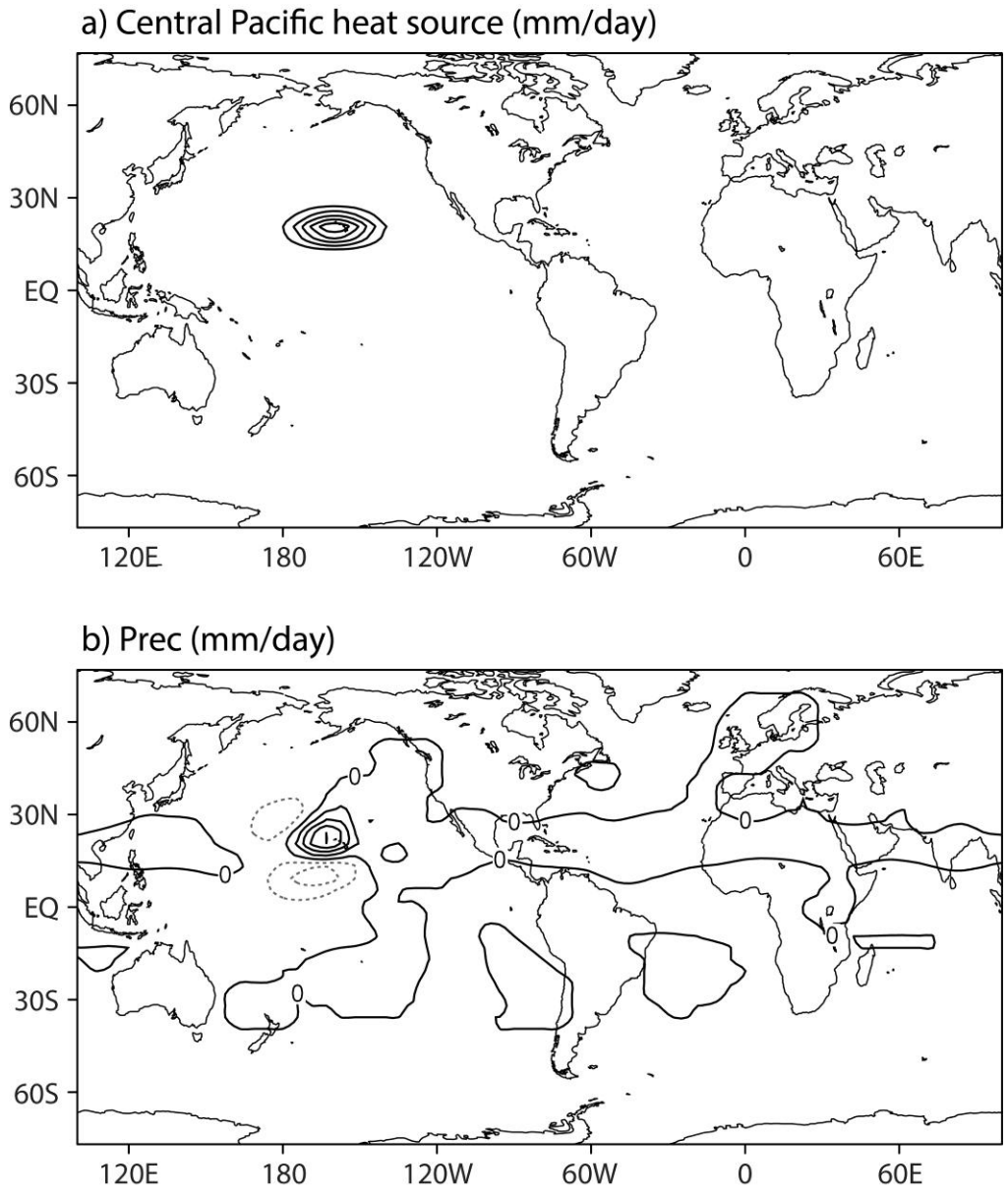

707

708 FIG. 6. (a) As in Fig. 1a, except shifting the heat source 90° in longitude to the central Pacific
709 region. (b) Precipitation anomalies in the central Pacific experiment in the QTCM. Negative
710 contour lines are dashed. The contour intervals are both 1mm/day.

711

712

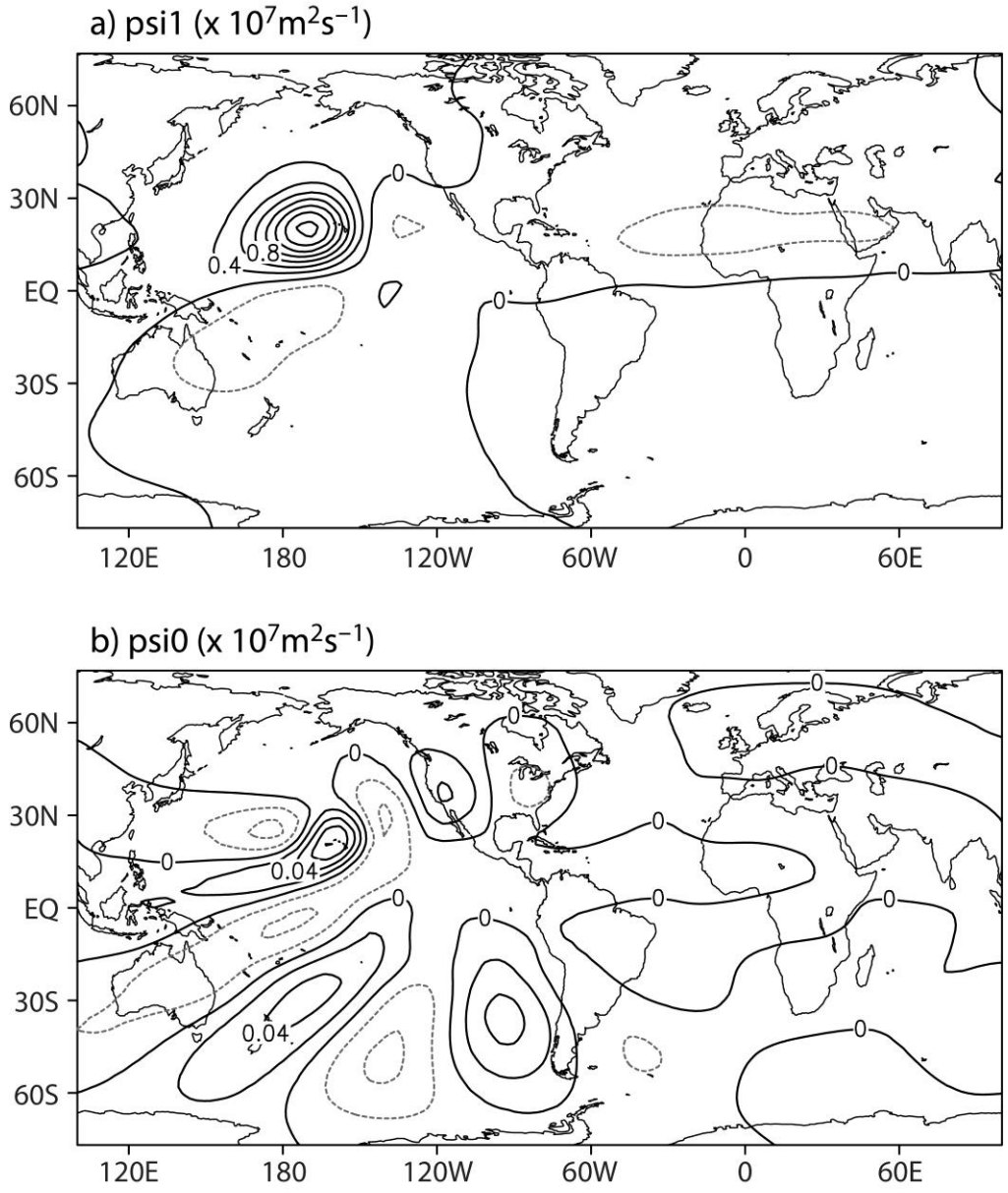

713

714 FIG. 7. The baroclinic streamfunction anomalies (a) and barotropic streamfunction anomalies (b)
715 in the central Pacific experiment in QTCM. Negative contour lines are dashed. The contour
716 intervals are 2 x 10^6 m^2 s^{-1} in (a) and 2 x 10^5 m^2 s^{-1} in (b).

717

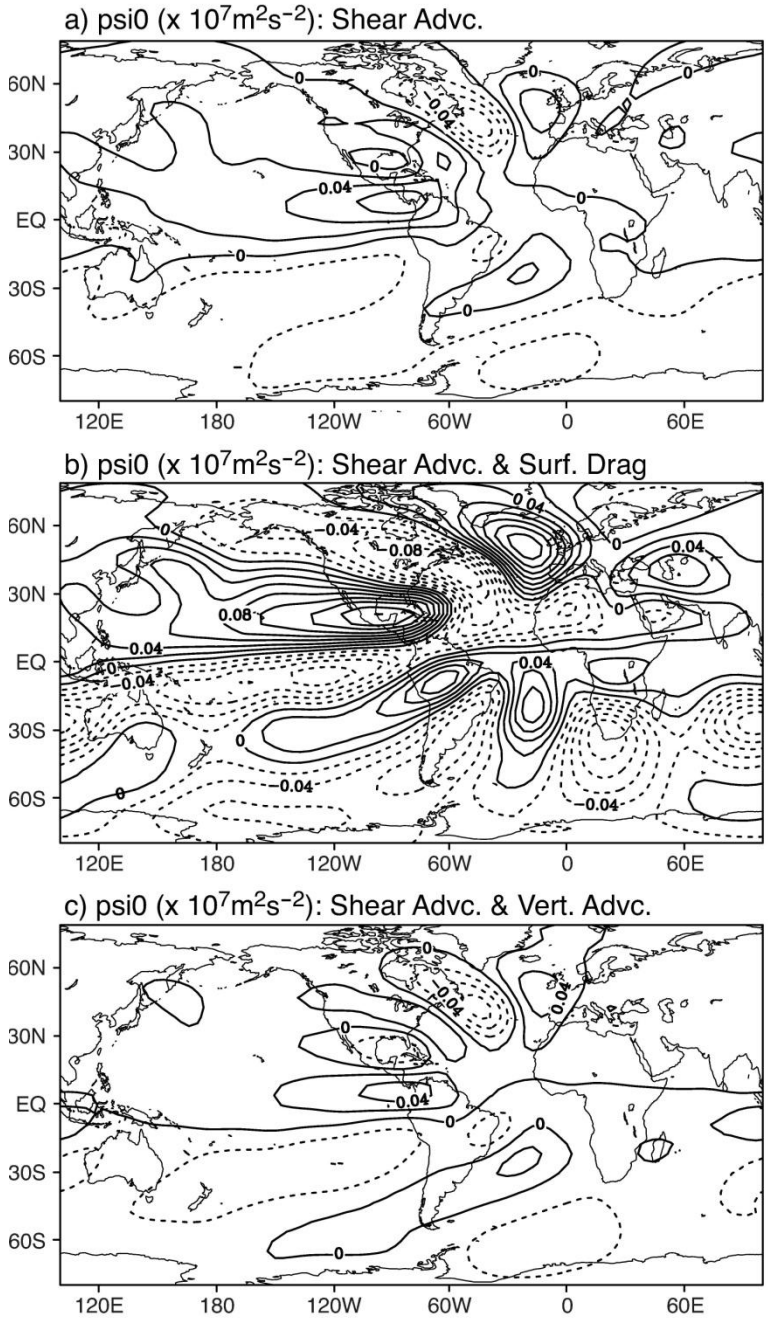

718

719 FIG. 8. The barotropic streamfunctions anomalies in the simple model AWP experiment (a) with
720 shear advection; (b) with shear advection and surface drag mechanisms; (c) with shear advection
721 and vertical advection mechanisms. Negative contour lines are dashed. The contour intervals are
722 2 x 10^5 m^2 s^{-1} in all three.